

Angle-dependent charge exchange and energy loss of slow highly charged ions in freestanding graphene

S. Creutzburg¹, A. Niggas², D. Weichselbaum², P. L. Grande³, F. Aumayr², and R. A. Wilhelm^{2,*}

¹*Helmholtz-Zentrum Dresden-Rossendorf, Institute of Ion Beam Physics and Materials Research, Bautzner Landstrasse 400, 01328 Dresden, Germany, EU*

²*TU Wien, Institute of Applied Physics, Wiedner Hauptstrasse 8-10/E134, 1040 Wien, Austria, EU*

³*Federal University of Rio Grande do Sul, Ion Implantation Laboratory, CEP 91501-970 Porto Alegre, Brazil*



(Received 13 July 2021; accepted 24 September 2021; published 11 October 2021)

The scattering of ions in solids is accompanied with momentum transfer and electronic excitations resulting in the slowing down of the ion. The amount of energy transferred in a single scattering event depends on the particular trajectory which can be traced back through the scattering angle. Performing scattering angle dependent measurements of slow highly charged Xe ions transmitted through freestanding single-, bi-, and trilayer graphene allows us to determine the charge exchange and energy loss for different minimal interatomic distances. Interestingly, the charge exchange shows an increase with scattering angle by a factor of less than 2, while the energy loss increases by more than a factor of 10 for 3° compared to forward direction. Our results can be compared to a time-dependent potential model and show that determination of the stopping cross section is not straightforward even with angle-dependent data at hand.

DOI: [10.1103/PhysRevA.104.042806](https://doi.org/10.1103/PhysRevA.104.042806)

I. INTRODUCTION

The evaluation of ion stopping cross sections from experiments is essential to verify theoretical [1–3] and semi-empirical models [4] and to serve then as important input parameter for the determination of the energy deposition in materials [5,6]. Applications of stopping data range from damage formation in first wall materials of nuclear fusion devices [7] to ion beam radiation therapy [8]. Ion induced damage is usually related to the *stopping power*, i.e., the *average* energy loss per unit path length. It is important to note in this respect, that the average is taken over all ion trajectories or in more quantitative terms: over all ion impact parameters or scattering angles [9]. However, in certain cases, i.e., using single crystalline target materials [10,11] or even two-dimensional (2D) materials [12,13], a trajectory selection can appear due to ion channeling or by using an angle-limited detector and experimental energy loss data will be sensitive to this selection. It is important not to confuse the typically angle-resolved or angle-limited experimental data with the energy loss cross section. It is common procedure to calculate the energy loss per unit path length from experimental data in transmission experiments by dividing the determined energy loss by the material thickness [14] and in backscattering experiments by dividing the energy width of a peak or plateau by twice the (effective) thickness of the material layer of interest [15,16]. This is only correct if no trajectory selection is present. Otherwise the partial stopping

cross section

$$S_{\text{part}} = 2\pi \int_{p_1}^{p_2} pT(p, E)dp \quad (1)$$

is actually determined, where the experiment measures the integral of transferred energies T per collision between the selected impact parameters p_1 and p_2 . Note that stopping power/force and stopping cross section are related only by the material density. In the case of plural and multiple scattering the estimation of the partial stopping cross section is more complex, but the general considerations still hold. Equation (1) yields the total stopping cross section only for $p_1 \rightarrow 0$ and $p_2 \rightarrow \infty$ at the same time. In solids the latter can be limited to a value close to the lattice constant.

In this work, we apply transmission spectroscopy of slow highly charged ions (HCIs) interacting with freestanding layers of graphene with 1, 2, and 3 atomic layers of thickness to shed more light on this fundamental problem. There exist theoretical calculations mostly for light ion scattering in graphene [3,17–21]. In this way we can explicitly address the regime of single, double, and multiple scattering in solids and see that the angle dependence of charge exchange vanishes already with 3 material layers. We use a rotatable, but acceptance angle-limited electrostatic analyzer in one experiment and an angle-resolved (position sensitive) detector in another experiment to detect transmitted heavy ions' charge state resolved up to the maximal scattering angle. We compare our data to a simulation which allows us to disentangle nuclear and electronic contributions to the energy loss and we conclude that the energy loss indeed increases significantly for larger deflection angles.

*Corresponding author: wilhelm@iap.tuwien.ac.at

II. EXPERIMENTAL AND MODELING METHODS

Ions were produced in electron beam ion traps (EBIT) from Dreebit GmbH, Germany [22]. One EBIT is located at the Helmholtz-Zentrum Dresden-Rossendorf (HZDR) and one at TU Wien (TUW). At HZDR the EBIT is mounted to an ultrahigh vacuum chamber holding a heatable target holder and a rotatable electrostatic analyzer with an acceptance angle of $\pm 0.5^\circ$ and an energy resolution of $\Delta E/E \approx 1.5 \times 10^{-3}$. HCIs are selected with the help of a Wien filter and the EBIT is biased to a negative potential to decelerate the ions when they are entering the experimental chamber. Details of this experiment can be found in Ref. [23].

At TUW the EBIT is connected to a time-of-flight (TOF) spectrometer, where samples are mounted on a heatable target holder. The beam is charge state selected by means of a Wien filter, focused and steered by a set of electrostatic lenses and deflection plates and cut in size to $0.5 \times 0.5 \text{ mm}^2$ with a vertical and horizontal slit in front of the sample (both 0.5 mm in size). Scattered ions are detected on a position sensitive Roentdek delay line detector (DLD) with an active area with the diameter of $\sim 40 \text{ mm}$. Charge states after sample transmission are analyzed by a DC voltage deflection field in combination with an additional horizontal slit (width 0.5 mm) encoding the charge state onto one position axis on the DLD. In addition the TOF is measured by detecting secondary electrons emitted from the sample as a start signal and the ion impact on the DLD as the stop signal. The energy resolution of the TOF is about 1%. All data is recorded in a listmode, which allows postprocessing of the data according to TOF or charge state filtering. A more detailed description of this setup can be found in Ref. [24]. The TOF detector can be rotated around the sample in transmission direction up to 8° , i.e., for higher scattering angles subsequent spectra are measured and stitched together to obtain larger scattering angle patterns (see Fig. 3).

In both experimental setups we apply ion fluences of $10^8 - 10^9 \text{ cm}^{-2}$ per spectrum and not more than 10^{11} cm^{-2} per sample to avoid sample damage to become severe. Note that the sputtering yield is still about 0.5 at the energies applied here [19], because of the absence of a collision cascade. The experimental results are compared to calculations based on the time-dependent potential (TDPot) model. Details can be found in Ref. [25]. Here a screened interaction potential between the ion and target atoms is used, which changes at every time step according to charge transfer and de-excitation rates taken from the classical over barrier model [26] and the interatomic Coulombic decay (ICD) process [27,28]. In this way, for a given target atomic geometry, each ion trajectory can be followed in time and the outgoing scattering angle, charge state and energy loss can be extracted. The latter is determined by momentum transfer to a target nucleus and inelastic losses due to the changing potential. Note, that in case of charge exchange and a nonconservative potential, nuclear and electronic losses are both inelastic. Electronic kinetic energy loss is determined by the difference between the ion's energy loss and the kinetic energies of all target atoms in the simulation cell.

Samples were commercially available freestanding single-layer graphene layers on a Quantifoil support acquired from

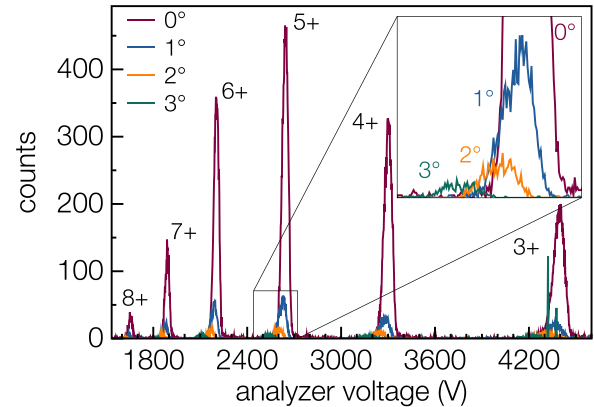


FIG. 1. Exit charge state spectra of Xe^{20+} , $E_{kin} = 75 \text{ keV}$ transmitted through freestanding single-layer graphene (SLG) for scattering angles up to 3° .

Graphenea. The base pressures in the target chambers are $1 \times 10^{-9} \text{ mbar}$. Samples were heated to 400°C prior to the experiment for about 12 h and kept at about 200°C during the experiments to avoid recontamination even under ultrahigh vacuum conditions. For a detailed description of the sample cleaning procedure (without laser exposure here), the reader is referred to Ref. [29]. Bilayer (BLG) and trilayer (TLG) graphene samples were also acquired from Graphenea and are produced there by manually stacking 2 or 3 layers of single-layer graphene (SLG) on top, respectively. Thus, the layer orientation is random. The samples are positioned at a normal incidence direction with respect to the incoming ion beam with an uncertainty of less than 1° , the relative orientation of the crystalline flakes of the graphene with respect to the ion beam is not controlled.

III. RESULTS

At HZDR Xe^{20+} ions at 75 keV kinetic energy were transmitted through a freestanding single layer of graphene. The corresponding spectra from the electrostatic analyzer can be seen in Fig. 1 for different observation angles. Under constant beam current conditions, one can see that the intensity of the transmitted ions decreases with increasing projectile scattering angle. Additionally, the peaks shift to lower analyzer voltages, which points to increasing energy loss at higher scattering angles. The mean outgoing charge state is about 5, which is well in agreement with what was observed previously [13,30] for HCI transmission through graphene. To evaluate the data from Fig. 1 further, we applied a deconvolution procedure, described in Ref. [31], which becomes necessary because peaks at larger charge exchange are broadened in an electrostatic analyzer.

The measured energy loss [panel (a)] and abundance [panel (d)] for the outgoing charge states of the Xe projectiles are shown in Fig. 2 (full circles) together with corresponding simulations based on the TDPot code (open triangles). The TDPot results are further separated in nuclear and electronic energy loss [panels (b) and (c)]. Symbol sizes in panels (a)–(c) correspond to the ion abundance. The total energy loss is weakly dependent on the exit charge state but increases by

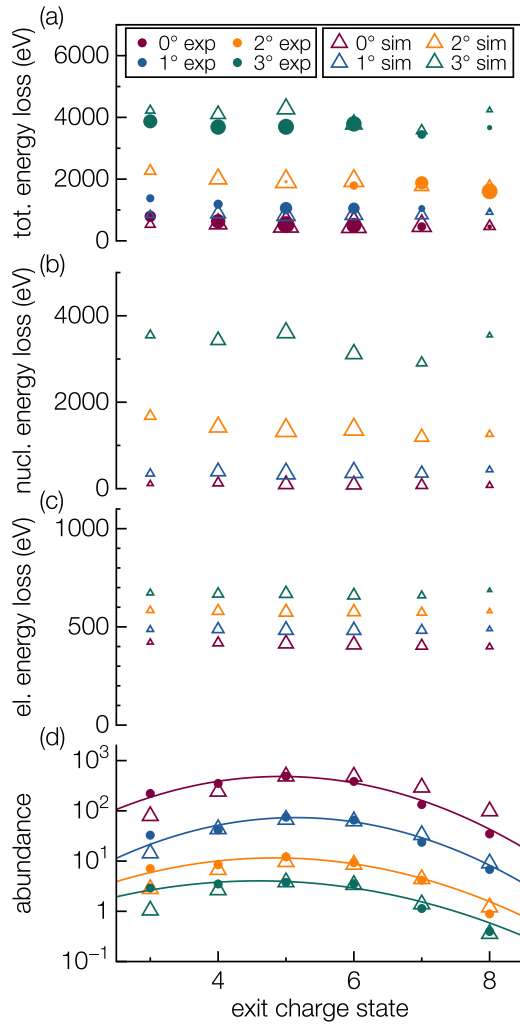


FIG. 2. (a) Measured total kinetic energy loss of Xe^{20+} at $E_{kin} = 75$ keV transmitted through freestanding single-layer graphene as a function of exit charge state. Values from the TDPot simulations are added for comparison. The symbol size represents the abundance of the respective charge states. (b) Nuclear and (c) electronic contributions to kinetic energy loss extracted from the simulations. (d) Ion's abundance as a function of exit charge state from experiments and simulations. The experimental data is fit by a Gaussian to extract the mean charge state.

more than a factor of 4 from 0° to 3° . The agreement between experimental data and simulation results is remarkably good. The nuclear energy loss contribution obtained from the simulations is small at around 100 eV under forward direction but increases by more than a factor of 30 to around 3200 eV at 3° . Note, that the maximal possible scattering angle of Xe on C is 5.34° . The relative increase of the simulated electronic energy loss is smaller, i.e., from about 400 eV by a factor of 1.7 to about 700 eV.

The exit charge state distributions in Fig. 2(d) (note the log scale) show a mean charge state of about 5.0 for 0° decreasing slightly to 4.6 for 3° . Again, simulation and experiment are in good agreement.

When using higher charge states of $q = 34$ and 38 as well as a higher kinetic energy of 166 keV at TUW, the exit

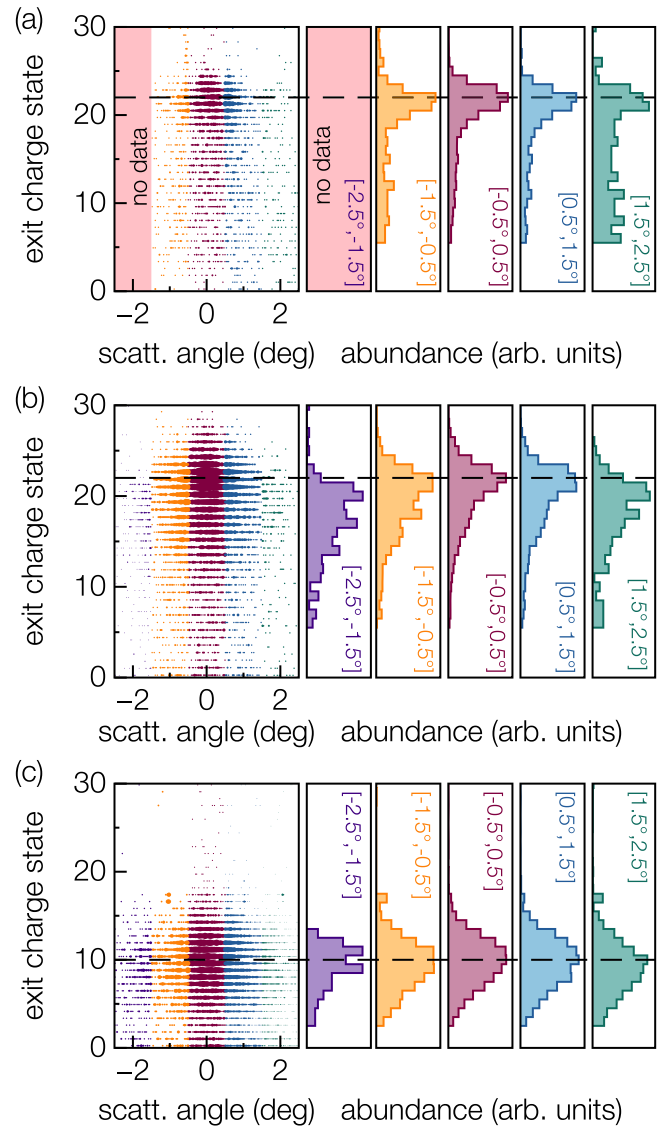


FIG. 3. (a) Charge state vs scattering angle plot for SLG where the data point sizes are according to the abundance in that bin. The differently colored regions are integrated over scattering angle ranges and the resulting charge state distributions are shown on the right. (b) and (c) are for BLG and TLG samples, respectively. (a) and (c) are for 166 keV Xe^{34+} ions and (b) for 166 keV Xe^{38+} ions.

charge state changes with scattering angle more significantly. Figure 3 shows examples of 2D charge state vs scattering angle data together with the exit charge state distributions for certain scattering angle ranges for SLG, BLG, and TLG. For the largest angles in the measurement, one can already see that the median of the distributions changes to smaller exit charge states.

The medians of the charge state distribution for the different scattering angles (mean values of the ranges indicated in Figs. 2 and 3) are plotted in Fig. 4. While for the low kinetic energy of 75 keV only a weak dependence can be seen, at higher kinetic energies and for the different target thicknesses, the charge exchange increases strongly with scattering angle.

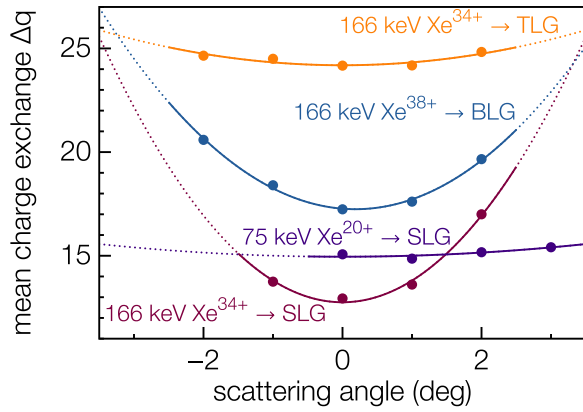


FIG. 4. Charge exchange $\Delta q = q_{in} - q_{out}$ dependence on scattering angle. The different target thicknesses and ion beam parameters are labeled. Each set of data is fitted with a quadratic function (as a guide to the eye), which is extrapolated (dotted line) to larger angles. Error bars are omitted since statistical errors are smaller than the point size and systematic errors cannot simply be quantified due to unknown detector efficiencies at different charge states, TOF-filter uncertainties, etc.

Further, the angular dependence is strongest for single layer graphene and becomes weaker for an increasing layer thickness.

To further elucidate on the energy loss dependence on the scattering angle, we extracted the closest approach of the ion to a target atom from the TDPot simulations for SLG samples taking the opening angle of the analyzer into account. Figure 5 shows the distributions of the closest approach for different observation angles for 75 keV Xe^{20+} ions. The mean of these distributions is marked as well.

Now, we can assign each scattering angle (i.e., observation angle) a (mean) closest approach, see Fig. 6. The maximal scattering angle of Xe on C is indicated by the dashed line. The skewed function (Moyal function) is fitted to the data as a guide to the eye, where the ion can not approach a carbon atom closer than 0.24 Å at 75 keV kinetic energy. At the

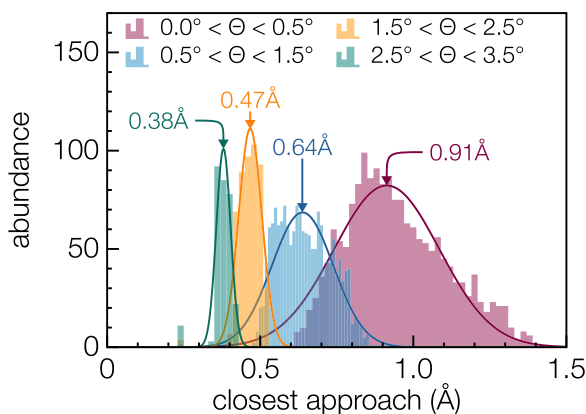


FIG. 5. TDPot result on ion abundance as a function of closest approach for scattering angles up to 3.5° from simulations for 75 keV Xe^{20+} transmitted through single-layer graphene. Mean values of the closest approach are indicated.

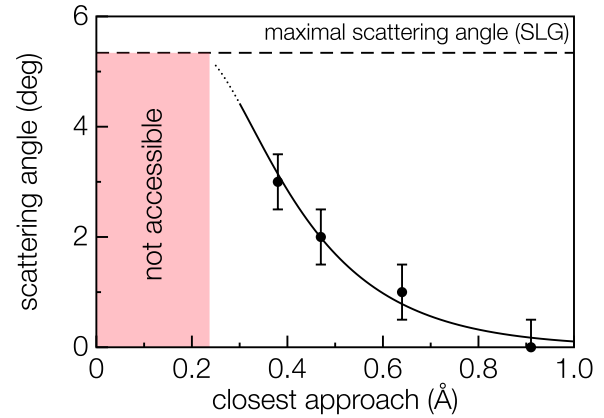


FIG. 6. Scattering angle as function of closest approach extracted from simulations for 75 keV Xe^{20+} on C. The maximal scattering angle for the present situation is indicated by the dashed line. The skewed fit is a guide to the eye.

present scattering angles between 0 and 3° we can now assign a closest approach between 0.3 and 1.0 Å.

Using this calibration, we plot the measured total kinetic energy loss from Fig. 2(a) as function of closest approach in Fig. 7. The measured data here is a weighted average for the different exit charge states. We can compare the experimental result now to an estimation based on the change in scattering potential. The interparticle interaction potential changes due to the inelasticity of the charge exchange process continuously on the way in and on the way out [25]. The total inelastic

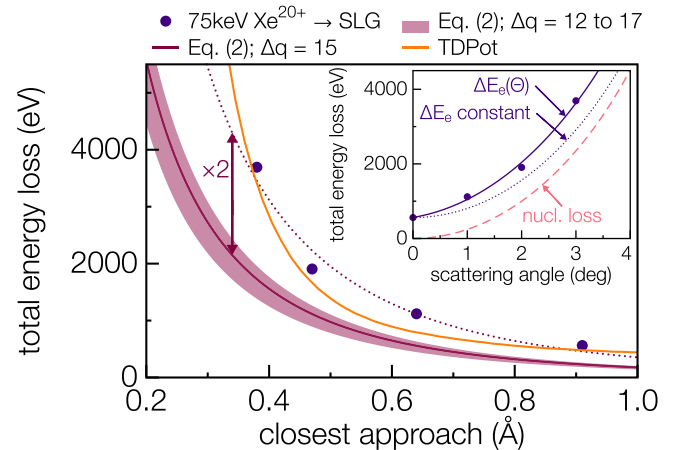


FIG. 7. Total measured energy loss as function of closest approach extracted from simulations for 75 keV Xe^{20+} in SLG. The data is compared to an estimation based on Eq. (2). The dotted line is the estimated energy loss multiplied by a factor of 2. The shaded area indicates the estimated energy loss for larger and smaller charge exchange based on the exit charge state distribution width in Fig. 2(d). The orange line is the result of the full TDPot simulation. The inset shows the experimentally determined total energy loss as function of scattering angle (purple). The data can be well reproduced by momentum transfer between the nuclei in a single collision including an angle dependent electronic energy loss (full line) taken from Fig. 2(c), see text. The nuclear loss contribution [bracket in Eq. (3)] is shown separately in light red.

energy loss of the system is then given in the center of mass system by the potential difference before and after the charge exchange at the position of closest approach as

$$\Delta V = \frac{\Delta q Z_2}{R_{\min}} \Phi(R_{\min}) = \Delta E_{\text{cms}}, \quad (2)$$

in atomic units where Δq is the final change in charge state, Z_2 is the atomic number of carbon, R_{\min} is the distance of closest approach and Φ is the interparticle screening function taking partial screening by the ion's core electrons into account. We use the Krypton-Carbon screening function here [32], while the particular choice of the screening function is of minor importance for the quantitative results. We can now compare the result of Eq. (2) to the experimental data in Fig. 7 and find a good agreement for $\Delta q = 15$ (mean charge exchange from experiment) taking an additional factor of 2 into account (dotted line). The screening lengths are chosen according to the definitions given in Ref. [25]. The general trend of the data is well reproduced, but the estimated energy loss is about a factor of 2 smaller than the experimental data. This discrepancy results from the neglect of target excitations in the estimation, i.e., taking the screening function Φ for a neutral target in its ground state. Still, the dependence on the closest approach is well reproduced. The full TDPot results shown in Figs. 2 and 7 take target excitations into account by a method described in Ref. [25]. Still, the simple estimation based on Eq. (2) already works well.

The total energy loss increases strongly for increasing scattering angle (see inset in Fig. 7) and decreasing closest approach. Purely elastic scattering would result in zero energy loss at 0° and the offset of 560 eV indicates already the presence of electronic stopping [cf. 2(c)]. The data in the inset of Fig. 7 can be fit with

$$\Delta E = E(1 - k_1^2(\cos \Theta \pm \sqrt{|k_2^2 - \sin^2 \Theta|})) + \Delta E_e(\Theta) \quad (3)$$

using $k_1 = \frac{m_1}{m_1 + m_2}$, $k_2 = \frac{m_2}{m_1}$ with ion mass m_1 and target mass m_2 , and E as the incident energy as well as Θ as scattering angle. The first term in Eq. (3) follows from nuclear scattering considering energy and momentum conservation. The two solutions follow from $m_1 > m_2$. The agreement with measured data can only be reached if the electronic energy loss $\Delta E_e(\Theta)$ is assumed to be (at least) linearly dependent on the scattering angle (full line) instead of a constant offset taken at 0° (dotted line), well in agreement with what can be seen in Fig. 2(c).

Figure 8 shows the energy loss for different 2D impact parameters in a SLG sample from the TDPot simulation. Different observation angles (and angular ranges) correspond to ions from different trajectories. At 3° the total energy loss increased by a factor of 6.6 compared to forward transmission, and the total area of impact parameters (i.e., the probability for these trajectories) decreased by a factor of 6.3. Even though smaller impact parameters are less likely (by a factor of 6.3 in this case), the energy loss increases at the same rate leading to a similar contribution to the total stopping cross section in Eq. (1).

Using purely the experimental energy loss data in Fig. 7 and assuming a straight line trajectory, i.e., $R_{\min} \approx p$, which is justified by the small scattering angles used here (in the

laboratory system), we can actually determine the energy transfer for a single collision (from a fit to experimental data), $T(p) \sim 339.6/p^{2.4} \text{ eV}\text{\AA}^{2.4}$ valid for $p > 0.24 \text{ \AA}$ and being significantly less steep than the $1/p^5$ dependence given by Firsov [33]. The partial stopping cross section for $0.24 \text{ \AA} < p < 1.47 \text{ \AA}$ then yields $5033 \text{ eV}\text{\AA}^2 = 503 \text{ eV}/(10^{15} \text{ atoms}/\text{cm}^2)$ according to Eq. (1). Note, that p cannot exceed 1.47 \AA in SLG. However, the $T(p)$ above shall not be used for smaller p as it diverges. We used $p_1 = 0.24 \text{ \AA}$ as this is the smallest R_{\min} for 75 keV Xe^{20+} on SLG in the straight line approximation. The full stopping cross section follows from $p_1 \rightarrow 0$, where we need to take deviations from the straight line trajectory into account according to $R_{\min} = \sqrt{(0.24 \text{ \AA})^2 + p^2}$. In the $T(R_{\min} = p)$ extracted from Fig. 7 above, we may substitute R_{\min} and deduce the full stopping cross section $S = 506 \text{ eV}/(10^{15} \text{ atoms}/\text{cm}^2)$, being only 0.5% larger than the partial cross section, which is clear from the way we expressed $R_{\min}(p)$.

Figure 7 shows also the result of the TDPot simulation, which yields a stopping cross section of $603 \text{ eV}/(10^{15} \text{ atoms}/\text{cm}^2)$.

The results above show that angle-resolved energy loss data is necessary to deduce a reliable value for the total stopping cross section. Our data up to 3° can be extrapolated to zero impact parameter and allows the determination of the stopping cross section, but it should be noted that the maximal scattering angle is 5.34° , i.e., close to our maximal angle in experiment. At different ion-to-target mass ratios more angles need to be measured, because the energy transfer per collision can follow a dependency on the impact parameter hard to predict from models especially when charge exchange is involved ($1/p^{2.4}$ in our case). Comparison with simulation results [e.g., TRIM as the standard code yields $210 \text{ eV}/(10^{15} \text{ atoms}/\text{cm}^2)$, but does not include any ion charge] should always consider the individual measurement geometry. It should be noted that the results here are obtained using highly charged ions, but the considerations regarding energy loss are valid for any charge state and any ion-to-target mass ratio.

IV. DISCUSSION

Our results show, that energy loss measurements of HCIs in forward direction are dominated by electronic losses, but at slightly larger angles nuclear losses start to dominate. Further, both nuclear and electronic losses depend on the ion trajectory, i.e., the particular scattering angle. Therefore, special care must be taken when comparing angle-resolved experimental data to simulation results, which typically yield angle-integrated data. This also implies that energy loss cross sections, i.e., impact parameter weighted average energy loss, cannot simply be extracted from angle-resolved measurements. The picture will change for thicker targets, where multiple scattering smears out all trajectory dependence and then each observation angle corresponds to, on average, very similar trajectories.

Another important result from Fig. 4 is the angular dependence of charge exchange. Here a clear material thickness and ion velocity dependence can be seen. Naturally, for SLG in the pure single scattering regime in comparison to thicker materials where more than one scattering event takes place

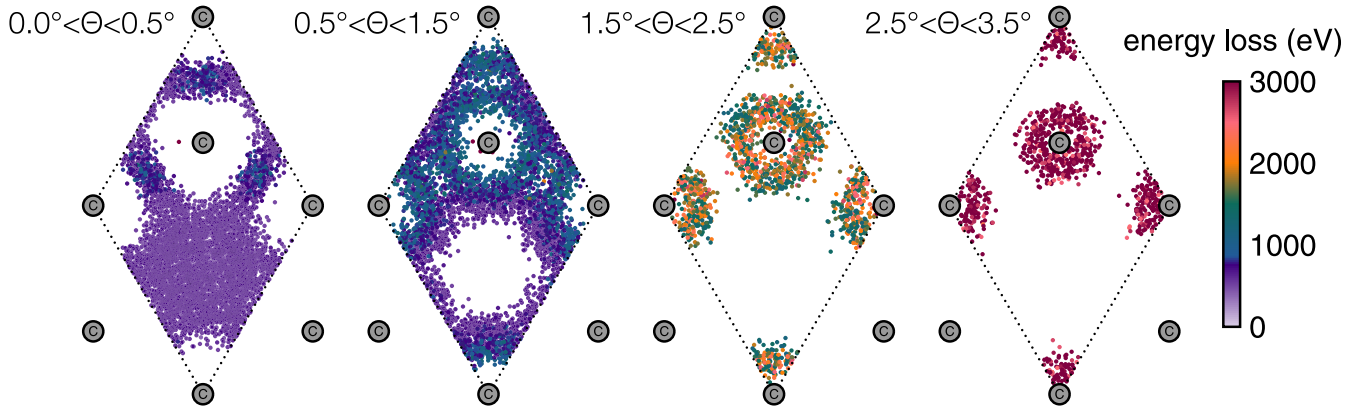


FIG. 8. 2D scatter plots for simulated trajectories of 75 keV Xe^{20+} ions through SLG for observation angle ranges. The energy loss is indicated by the color scale. The target atom positions are indicated by the grey symbols and the dotted line indicates the range of impact parameters chosen.

on the way through the material, the trajectory dependence is strongest. With increasing material thickness multiple scattering smears out the angular dependence, because an intrinsic averaging over different impact parameters occurs. Already about three scattering events (cf. TLG) seem to be enough to assume a trajectory independence. Consequently, the ion-exit charge state distribution for TLG is closer to a Gaussian [cf. Fig. 3(c)] as expected from the central limit theorem as the number of layers increases. Further, at larger kinetic energies the ion approaches the target nuclei closer, i.e., for a given impact parameter p the closest approach R_{\min} is smaller but also the total transmission time is smaller. Interatomic energy exchange leading to the stabilization of resonantly captured electrons by ICD shows a saturation of the ICD rate at interatomic separations about smaller than the lattice constant of graphene (1.4 Å) [25,30]. Thus, we do not assume the ICD rate to be dependent on the closest approach, but rather that at larger kinetic energies the time the ion spends in the ICD active region around a target atom is too small for ICD to fully de-excite the ion. The interaction time is naturally also impact parameter dependent [34]¹, leading to the angular dependence in Fig. 4. Yet, at the smaller kinetic energy of 75 keV the interaction time exceeds the ICD lifetime for all trajectories and thus ICD is efficient for de-excitation for all trajectories. As discussed already in Ref. [28], deep lying atomic states in the ion may not be populated by ICD in any case, because of the small wave function overlap with these core states. Then, some excitation energy remains in the projectile on the way out and intra-atomic Auger de-excitation further leads to the filling of the core states by ejection of some Auger electrons. The result is an angle independent charge exchange

distribution, where the, on average, remaining charge stems from the Auger electron emission after transmission.

V. CONCLUSION

We showed that HCIs transmitted through single-, bi-, and trilayer graphene exhibit a strong angular dependence of the observed charge exchange for larger kinetic energies and thin samples. Thicker samples or reduced kinetic energies lead to a weaker angular dependence. A strong dependence of the energy loss on scattering angle is also observed even for the smallest kinetic energy in our study. The charge exchange can be understood by the trajectory dependent transmission time through a material layer. The energy loss at larger angles is a result of momentum transfer to target nuclei, i.e., nuclear stopping. Both nuclear and electronic stopping are enhanced by a factor 2 to 3 due to the incident charge state [25,35] in contrast to estimations given by established models which neglect the ion charge state. Using a simple estimation for the energy loss based on the change in scattering potential due to charge exchange, cf. Eq. (2), we can reproduce our experimental data well within a factor of 2 neglecting inelastic losses due to target atom excitation.

ACKNOWLEDGMENTS

We acknowledge funding from the Austrian FWF through Projects No. Y1174-N36 and No. I4914-N. Part of this research was carried out at the Ion Beam Center at the Helmholtz-Zentrum Dresden-Rossendorf e.V., a member of the Helmholtz Association. This work has been carried out within the framework of the EUROfusion Consortium and has received funding from the Euratom research and training programme 2014-2018 and 2019-2020 under Grant agreement No. 633053. The views and opinions expressed herein do not necessarily reflect those of the European Commission. P.L.G. acknowledges funding by the Alexander-von-Humboldt (AvH) foundation.

¹The interaction time can be defined as $t = p/v$ similarly to the definition of Bohr's adiabatic radius $p = v/\omega$, where ω is the transmission frequency (passing one target atom) and a maximal contributing impact parameter can be estimated from $\omega = \omega_0$, where ω_0 is the mean electron orbital frequency of the target atoms.

- [1] G. Schiwietz and P. L. Grande, A unitary convolution approximation for the impact-parameter dependent electronic energy loss, *Nucl. Instrum. Methods Phys. Res., Sect. B* **153**, 1 (1999).
- [2] A. Schinner and P. Sigmund, Expanded PASS stopping code, *Nucl. Instrum. Methods Phys. Res., Sect. B* **460**, 19 (2019).
- [3] A. Schleife, Y. Kanai, and A. A. Correa, Accurate atomistic first-principles calculations of electronic stopping, *Phys. Rev. B* **91**, 014306 (2015).
- [4] J. F. Ziegler, M. Ziegler, and J. Biersack, SRIM—The stopping and range of ions in matter (2010), *Nucl. Instrum. Methods Phys. Res., Sect. B* **268**, 1818 (2010).
- [5] M. V. Moro, P. Bauer, and D. Primetzhofer, Experimental electronic stopping cross section of transition metals for light ions: Systematics around the stopping maximum, *Phys. Rev. A* **102**, 022808 (2020).
- [6] W. J. Weber and Y. Zhang, Predicting damage production in monoatomic and multi-elemental targets using stopping and range of ions in matter code: Challenges and recommendations, *Curr. Opin. Solid State Mater. Sci.* **23**, 100757 (2019).
- [7] S. Brezinsek, J. Coenen, T. Schwarz-Selinger, K. Schmid, A. Kirschner, A. Hakola, F. Tabares, H. van der Meiden, M.-L. Mayoral, M. Reinhart, E. Tsitrone, T. Ahlgren, M. Aints, M. Airila, S. Almaviva, E. Alves, T. Angot, V. Anita, R. Arredondo Parra, F. Aumayr *et al.*, Plasma-wall interaction studies within the EUROfusion consortium: Progress on plasma-facing components development and qualification, *Nucl. Fusion* **57**, 116041 (2017).
- [8] M. Durante and H. Paganetti, Nuclear physics in particle therapy: A review, *Rep. Prog. Phys.* **79**, 096702 (2016).
- [9] P. Sigmund and A. Schinner, Note on measuring electronic stopping of slow ions, *Nucl. Instrum. Methods Phys. Res., Sect. B* **410**, 78 (2017).
- [10] S. Lohmann and D. Primetzhofer, Disparate Energy Scaling of Trajectory-Dependent Electronic Excitations for Slow Protons and He Ions, *Phys. Rev. Lett.* **124**, 096601 (2020).
- [11] A. Hentz, G. S. Parkinson, P. D. Quinn, M. A. Muñoz-Márquez, D. P. Woodruff, P. L. Grande, G. Schiwietz, P. Bailey, and T. C. Q. Noakes, Direct Observation and Theory of Trajectory-Dependent Electronic Energy Losses in Medium-Energy Ion Scattering, *Phys. Rev. Lett.* **102**, 096103 (2009).
- [12] R. A. Wilhelm, E. Gruber, R. Ritter, R. Heller, S. Facsko, and F. Aumayr, Charge Exchange and Energy Loss of Slow Highly Charged Ions in 1 nm Thick Carbon Nanomembranes, *Phys. Rev. Lett.* **112**, 153201 (2014).
- [13] E. Gruber, R. A. Wilhelm, R. Pétuya, V. Smejkal, R. Kozubek, A. Hierzenberger, B. C. Bayer, I. Aldazabal, A. K. Kazansky, F. Libisch, A. Krasheninnikov, M. Schleberger, S. Facsko, A. G. Borisov, A. Arnau, and F. Aumayr, Ultrafast electronic response of graphene to a strong and localized electric field, *Nat. Commun.* **7**, 13948 (2016).
- [14] D. Goebel, K. Khalal-Kouache, D. Roth, E. Steinbauer, and P. Bauer, Energy loss of low-energy ions in transmission and backscattering experiments, *Phys. Rev. A* **88**, 032901 (2013).
- [15] S. N. Markin, D. Primetzhofer, M. Spitz, and P. Bauer, Electronic stopping of low-energy H and He in Cu and Au investigated by time-of-flight low-energy ion scattering, *Phys. Rev. B* **80**, 205105 (2009).
- [16] P. Bauer, How to measure absolute stopping cross sections by backscattering and by transmission methods, *Nucl. Instrum. Methods Phys. Res., Sect. B* **27**, 301 (1987).
- [17] C. Brand, M. Debiassac, T. Susi, F. Aguilon, J. Kotakoski, P. Roncin, and M. Arndt, Coherent diffraction of hydrogen through the 246 pm lattice of graphene, *New J. Phys.* **21**, 033004 (2019).
- [18] A. Kononov and A. Schleife, Anomalous Stopping and Charge Transfer in Proton-Irradiated Graphene, *Nano Lett.* **21**, 4816 (2021).
- [19] O. Lehtinen, J. Kotakoski, A. V. Krasheninnikov, A. Tolvanen, K. Nordlund, and J. Keinonen, Effects of ion bombardment on a two-dimensional target: Atomistic simulations of graphene irradiation, *Phys. Rev. B* **81**, 153401 (2010).
- [20] A. Ojanperä, A. V. Krasheninnikov, and M. Puska, Electronic stopping power from first-principles calculations with account for core electron excitations and projectile ionization, *Phys. Rev. B* **89**, 035120 (2014).
- [21] M. Čosić, S. Petrović, and N. Nešković, The forward rainbow scattering of low energy protons by a graphene sheet, *Nucl. Instrum. Methods Phys. Res., Sect. B* **422**, 54 (2018).
- [22] G. Zschornack, M. Kreller, V. P. Ovsyannikov, F. Grossman, U. Kentsch, M. Schmidt, F. Ullmann, and R. Heller, Compact electron beam ion sources/traps: Review and prospects (invited), *Rev. Sci. Instrum.* **79**, 02A703 (2008).
- [23] S. Creutzburg, J. Schwestka, A. Niggas, H. Inani, M. Tripathi, A. George, R. Heller, R. Kozubek, L. Madauß, N. McEvoy, S. Facsko, J. Kotakoski, M. Schleberger, A. Turchanin, P. L. Grande, F. Aumayr, and R. A. Wilhelm, Vanishing influence of the band gap on the charge exchange of slow highly charged ions in freestanding single-layer MoS₂, *Phys. Rev. B* **102**, 045408 (2020).
- [24] J. Schwestka, D. Melinc, R. Heller, A. Niggas, L. Leonhartsberger, H. Winter, S. Facsko, F. Aumayr, and R. Wilhelm, A versatile ion beam spectrometer for studies of ion interaction with 2D materials, *Rev. Sci. Instrum.* **89**, 085101 (2018).
- [25] R. Wilhelm and P. Grande, Unraveling energy loss processes of low energy heavy ions in 2D materials, *Commun. Phys.* **2**, 89 (2019).
- [26] J. Burgdörfer, P. Lerner, and F. W. Meyer, Above-surface neutralization of highly charged ions: The classical over-the-barrier model, *Phys. Rev. A* **44**, 5674 (1991).
- [27] L. S. Cederbaum, J. Zobeley, and F. Tarantelli, Giant Intermolecular Decay and Fragmentation of Clusters, *Phys. Rev. Lett.* **79**, 4778 (1997).
- [28] R. A. Wilhelm, E. Gruber, J. Schwestka, R. Kozubek, T. I. Madeira, J. P. Marques, J. Kobus, A. V. Krasheninnikov, M. Schleberger, and F. Aumayr, Interatomic Coulombic Decay: The Mechanism for Rapid Deexcitation of Hollow Atoms, *Phys. Rev. Lett.* **119**, 103401 (2017).
- [29] A. Niggas, J. Schwestka, S. Creutzburg, T. Gupta, D. Eder, B. C. Bayer, F. Aumayr, and R. Wilhelm, The role of contaminations in ion beam spectroscopy with freestanding 2D materials: A study on thermal treatment, *J. Chem. Phys.* **153**, 014702 (2020).
- [30] A. Niggas, S. Creutzburg, J. Schwestka, B. Wockinger, T. Gupta, P. L. Grande, D. Eder, J. P. Marques, B. C. Bayer, F. Aumayr, R. Bennett, and R. A. Wilhelm, Peeling graphite layer by layer reveals the charge exchange dynamics of ions inside a solid, *Commun. Phys.* **4**, 180 (2021).

- [31] R. A. Wilhelm, E. Gruber, R. Ritter, R. Heller, A. Beyer, A. Turchanin, N. Klingner, R. Hübner, M. Stöger-Pollach, H. Vieker, G. Hlawacek, A. Götzhäuser, S. Facsko, and F. Aumayr, Threshold and efficiency for perforation of 1 nm thick carbon nanomembranes with slow highly charged ions, *2D Mater.* **2**, 035009 (2015).
- [32] W. D. Wilson, L. G. Haggmark, and J. Biersack, Calculations of nuclear stopping, ranges, and straggling in the low-energy region, *Phys. Rev. B* **15**, 2458 (1977).
- [33] O. B. Firsov, A qualitative interpretation of the mean electron excitation energy in atomic collisions, *Sov. Phys. JETP-USSR* **36**, 1076 (1959).
- [34] P. Sigmund, *Particle Penetration and Radiation Effects*, Springer Series in Solid-State Sciences Vol. 151 (Springer, Berlin, 2006), p. 449.
- [35] T. Schenkel, A. Hamza, A. Barnes, and D. Schneider, Interaction of slow, very highly charged ions with surfaces, *Prog. Surf. Sci.* **61**, 23 (1999).